Electrocatalysis (2019) 10:173–183
https://doi.org/10.1007/s12678-019-0506-6

ORIGINAL RESEARCH

Influence of Surface Treatment on the Kinetics of the Hydrogen Evolution Reaction on Bulk and Porous Nickel Materials

Michał Grdeń [1,2] · Gregory Jerkiewicz [3]

Published online: 1 February 2019

Abstract

The hydrogen evolution reaction (HER) occurring at porous Ni foam (Incofoam) and bulk polycrystalline Ni electrodes in 0.50 M aqueous KOH solution is studied at low overpotentials (down to − 0.35 V vs. RHE) in the $277 \leq T \leq 308$ K range. The experiments are conducted using "as received" and chemically etched Ni foams as well as polished and chemically etched polycrystalline Ni rods for comparative analysis. The chemical etching removes the oxide/hydroxide layer from the material's surface and modifies its morphology. Scanning electron microscopy and X-ray photoelectron spectroscopy are employed to examine the surface morphology and the surface chemical composition of the Ni foam prior to and after the chemical etching. Cyclic voltammetry and steady-state Tafel polarization measurements are conducted to analyze the electrochemical behavior of the Ni materials. It is found that the electrocatalytic activity of Ni materials towards the HER depends on the material's pre-treatment. The electrodes subjected to the chemical etching exhibit higher values of the Tafel slope and the exchange current density as compared to non-etched surfaces. The most pronounced effect is observed for the etched Ni foam for which the pre-treatment also affects the activation energy. This behavior is attributed to the removal of surface oxides/hydroxides and to surface roughening brought about by the "chemical etching." Together, these results reveal that the mechanism of the HER depends on the morphology and chemical state of the Ni material. In addition, it shows that suitable surface treatment can decrease the overpotential required to achieve a desired reaction rate (current density).

Keywords Nickel foam · Polycrystalline nickel · Chemical etching · Hydrogen evolution reaction · Tafel plots · Activation energy

Introduction

Porous metallic and carbon-based materials, such as foams, offer many structural advantages (e.g., high surface area, open-pore structure, low density) that make them suitable materials for applications in electrochemical and non-electrochemical technologies. Carbon-based foams are typically used as a support and a current collector on which electroactive material is deposited [1, 2]. Metallic foams fulfill several requirements and act simultaneously as a current collector and an electroactive material. Their electrocatalytic activity can be enhanced through a suitable surface treatment and/or addition of catalytically highly active materials. If the surface modifiers are platinum group metals (PGMs), then they are often employed in the form of nanoparticles [3]. Some of the most common electrochemical applications of metallic and carbon-based foams include flow-through cells [4], batteries [1, 2], water electrolyzers and electrocatalytic systems [3–9], and specialized setups for spectroscopic measurements under electrochemical conditions (e.g., optically transparent electrodes) [10, 11].

Nickel is one of the most frequently used metals to manufacture metallic foams. It is due to several properties, such as relatively high (electro)catalytic activity, high corrosion stability in alkaline and neutral aqueous media, abundance, and low cost. Nickel is also one of the most important metals and is used to prepare various metallic alloys. For instance, Ni-containing stainless steels and superalloys are used as

✉ Michał Grdeń
mgrden@chem.uw.edu.pl

✉ Gregory Jerkiewicz
gregory.jerkiewicz@queensu.ca

[1] Faculty of Chemistry, University of Warsaw, Pasteura 1, 02-093 Warsaw, Poland

[2] Biological and Chemical Research Centre, University of Warsaw, Żwirki i Wigury 101, 02-089 Warsaw, Poland

[3] Department of Chemistry, Queen's University, Kingston, Ontario K7L 3N6, Canada

construction materials; nickel-rich intermetallic compounds are used in hydrogen storage systems and nickel-metal hydride batteries; and nickel-titanium shape-memory alloys are commonly used in dentistry as archwires.

Commercial Ni foams are manufactured using open-cell polyurethane foam that acts as a template on which a thin layer of nickel is deposited by chemical vapor deposition (CVD) or physical vapor deposition (PVD) using the nickel carbonyl process. The thickness of the Ni deposit is increased either by continuing CVD/PVD or using electrodeposition. At the end, the polyurethane template is removed by sintering and the final product is a pure Ni foam [12]. The application of different polyurethane foam templates facilitates control of the strut thickness and pore size, which is typically in the 450–3200-μm range [12].

In the emerging hydrogen economy, hydrogen gas is the energy carrier that is produced by water electrolysis using renewable energy sources (e.g., hydroelectricity, solar energy, wind power). Such produced hydrogen gas can then be used in fuel cells to generate electrical and thermal energies. These technologies stimulate interest in electrochemical processes involving hydrogen, such as the hydrogen evolution reaction (HER) and the hydrogen oxidation reaction (HOR). The HER taking place in alkaline water electrolyzers is one of the most important electrocatalytic processes, where Ni-containing electrodes are applied [6, 13–16]. Although Ni is less active than noble metals (e.g., Pd, Pt, Rh, or Ir) towards the HER [6, 17], it is the most abundant non-noble metal that shows high electrocatalytic activity towards the process. The electrocatalytic activity of a material towards a given electrochemical reaction is typically examined by measuring the current (I) or current density (j) as a function of the overpotential (η). Then, a Tafel plot (a plot of log j or log I versus η) is constructed, on the basis of which the exchange current (I_o) or current density (j_o) as well as the Tafel slope (b) are determined. The Tafel slope for the HER taking place in alkaline aqueous media at Ni materials and at the room temperature reported by majority of authors in the low overpotential region is ca. 116–117 mV dec^{-1} [18–31]. However, lower values (e.g., < 100 mV dec^{-1}) as well as higher values (e.g., > 140 or higher mV dec^{-1}) of the Tafel slope are sometimes reported for Ni materials having various forms, such as bulk Ni, porous Ni, and Raney Ni [5, 8, 21, 28, 32–40]. As regards the reaction mechanism, it is known to follow the Volmer-Tafel mechanism [24, 29, 33, 34, 41–43], the Volmer-Heyrovsky mechanism [18–20, 23, 26, 27, 44], or a mixed mechanism involving both these pathways [45].

An analysis of the j_o values for the HER taking place at Ni materials in alkaline aqueous media is often complicated, because they are not always reported with respect to the real electrode surface area (A_r) [7, 27, 46]. In fact, in situ determination of A_r or the electrochemically active surface area (A_{ecsa}) of Ni materials is a challenging task, because it requires a probing species that interacts with every Ni surface atom. Elsewhere, it was proposed that the value of A_r or A_{ecsa} of Ni materials in alkaline aqueous media can be determined by analyzing the charge associated with the formation of α-$Ni(OH)_2$ [18, 27, 38, 47, 48] or the charge associated with the formation and reduction of NiOOH in the presence of oxalates (the so-called oxalate method) [49, 50]. Another approach is based on the measurement of the double-layer capacitance [19, 46–48, 51, 52]. The most frequently reported value of j_o for the HER taking place at Ni materials is j_o = 6.3 μA cm^{-2}, and this value is used in the construction of the electrochemical volcano plot for the HER [6, 17, 53].

In this contribution, we analyze the influence of the pre-treatment of bulk and foam-shaped Ni materials on the kinetics of the HER in aqueous KOH solution. The pre-treatment of bulk Ni materials involves polishing and chemical etching, while the Ni foams are analyzed as received or chemically etched. The applied chemical etching of Ni foams is gentle and removes a surface passive layer while preserving the macroscopic structure. The experimental work is conducted at various temperatures with the objective of determining the apparent activation energy of the process. The novel results reported in this contribution demonstrate that the surface pre-treatment significantly affects the intrinsic electrocatalytic activity of the Ni material towards the HER. They lead to an important observation that any analysis of the electrocatalytic activity of Ni materials requires knowledge of their surface chemical state, thus their surface chemical composition.

Experimental

Because the experimental conditions employed in the course of research were similar to those reported elsewhere [47], only the main aspects of the experimental work are described below. The experiments were carried out in a Pyrex glass, three-compartment cell, thus with separate working, reference, and counter electrode compartments. Platinum foil was used as a counter electrode, while the reference electrode was a reversible hydrogen electrode (RHE) in the form of platinized Pt foil. Ultra-high-purity H_2(g) (99.999% in purity) pre-saturated with high-purity water vapor was passed through the reference electrode compartment at a pressure of 1.00 atm. All potential values in the contribution are reported with respect to the RHE. The experiments were carried out in 0.50 M aqueous KOH (Sigma-Aldrich) solution outgassed using ultra-high-purity N_2(g) (99.999% in purity). All solutions were prepared using ultra-high-purity water (Millipore, 18.2 MΩ cm in resistivity) and were pre-electrolyzed for several hours to remove traces of any remaining metals. Two types of nickel materials were examined: polycrystalline, bulk rod (5.00 mm in diameter, Alfa Aesar Puratronic, 99.999% in purity) and a Ni foam (Incofoam®) supplied by INCO

Technical Services [12, 47, 54]. Incofoam had an open-pore structure with small and large open pores, ca. 50 ± 10 μm and 500 ± 100 μm in size, as determined using scanning electron microscopy (Fig. 1) [47]. Samples of the Ni foam were cut out of Incofoam sheets and had a square shape; their thickness was 1.00 mm and their mass was consistently in the 0.02–0.03-g range (each sample was weighed prior to performing experiments). A fine Ni wire (99.999% in purity) was weaved in the top edge of a Ni foam sample for electrical contact; its A_r was negligible compared to that of the Ni foam sample. Each Ni foam sample was degreased in acetone under reflux (for at least 30 min) and then repetitively rinsed using ultra-high-purity water; the final step involved rinsing with water under sonication conditions. The Ni foam sample prepared using this procedure is referred to as "as received." The preparation of "chemically etched" samples involved the following additional steps: (i) chemical etching in a solution containing 30 cm^3 HNO_3, 10 cm^3 H_2SO_4, 10 cm^3 H_3PO_4, and 50 cm^3 glacial CH_3COOH [47, 49, 55, 56] for 2 min at the room temperature [47] and (ii) rinsing in ultra-high-purity water as described above. As reported elsewhere, the chemical etching removes the native surface oxide/hydroxide layer and increases the surface roughness by ca. 50% [47]. Examples of X-ray photoelectron (XPS) spectra acquired for the as-received and chemically etched foams are shown in Fig. 2a, b. The XPS analysis focuses on the Ni($2p_{3/2}$) peak and respective satellite peaks. Removal of the surface oxides/hydroxides gives rise to an increase of the intensity of the metallic peak (Ni(0)) at a binding energy (*BE*) of 852.7 eV [57] and a decrease in the Ni(2+) signal at 855.9 eV. The latter peak is broad and poorly defined, and most likely contains contributions from $Ni(OH)_2$ (*BE* = 855.7 eV) [57] and NiO (*BE* = 853.7 eV) [57]. The satellite peaks at binding energies of 860.9 eV, 861.5 eV, and 858.7 eV are due to the presence of NiO, $Ni(OH)_2$, and Ni in the surface region of the foams [57]. It is important to mention

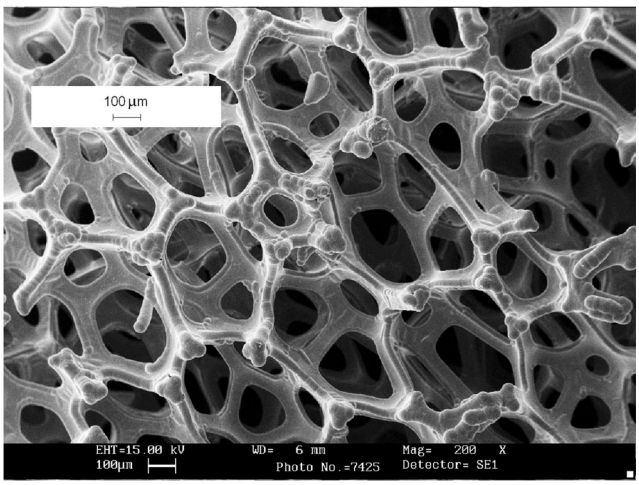

Fig. 1 SEM micrograph of a Ni foam obtained at a magnification of 200×

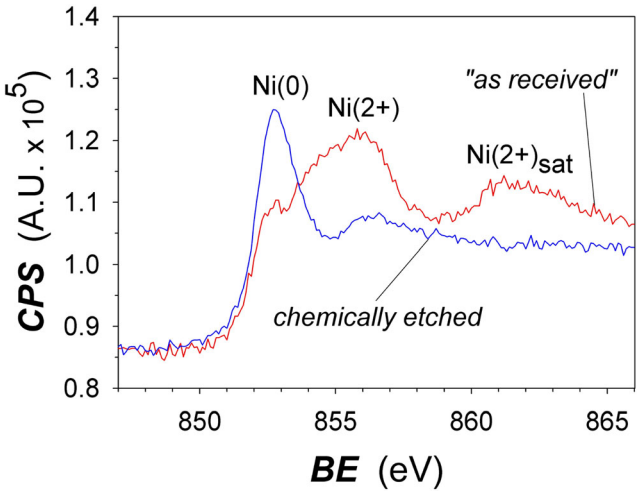

Fig. 2 XPS spectra for the Ni($2p_{3/2}$) band and its satellites for the as-received Ni foam and the chemically etched Ni foam

that some of these features overlap. In the case of the chemically etched surface, the presence of residual Ni oxides/hydroxides is due to incomplete removal of the oxides/hydroxides by the etching or due to re-oxidation of the surface prior to the XPS measurements. Scanning electron microscopy (SEM) micrographs shown in Fig. 3a, b reveal that application of the "chemical etching" also modifies the foam surface by increasing its roughness and by forming nanostructures within local surface regions. A high-purity (99.999%), polycrystalline Ni rod sealed in a Teflon sleeve served as a bulk Ni electrode [47, 54, 58, 59]. When used as a "polished" bulk electrode, it was mechanically polished with alumina (down to 0.05 μm, Buehler Micropolish) to a mirror-like finish followed by thorough rinsing with ultra-high-purity water. Its surface roughness was $R = 2.1$ due to remaining nano-roughness and surface curvature ($R = A_r/A_{geom}$, where A_{geom} is the geometric surface area, thus a two-dimensional projection of the three-dimensional surface). When used as a chemically etched bulk electrode, it was mechanically polished as described above, rinsed, and chemically etched in the above-mentioned solution for 2 min. The chemical etching was followed by thorough rinsing [47]. The chemical etching increased the surface roughness which was found to be $R = 3.0$ [47].

Kinetic studies of the HER were preceded by the electrode conditioning by applying repetitive potential cycling (typically 50 cycles) between − 0.15 and 0.50 V at a potential scan rate of $s = 100$ mV s^{-1}, thus in the range of formation and reduction of α-$Ni(OH)_2$. The final cycle was negative-going and created a metallic electrode surface [60, 61]. The procedure used to measure Tafel plots is presented in Fig. 4 [62]. The pre-treatment involved the application of an initial potential of $E_i = 0.100$ V for a short period of time, typically in the 60–120-s range, and then a given final potential (E_f) in the HER range ($-0.35 \le E_f \le -0.05$ V); each chronoamperometry measurement at E_f lasted until a steady-state current was

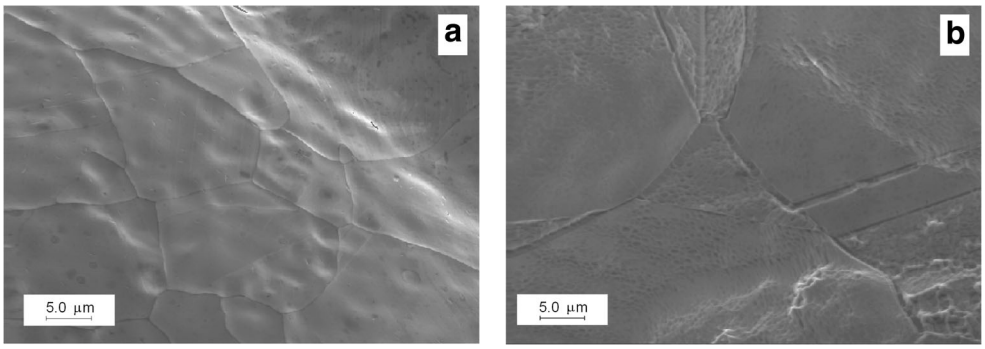

Fig. 3 SEM micrographs acquired at a magnification 2500× for **a** the as-received Ni foam and **b** the chemically etched Ni foam

measured (up to several hundred seconds). A comparison of HER current values recorded prior to and after application of the potential program depicted in Fig. 4 shows that the electrodes were fairly stable during the HER experiments, which lasted up to ca. 1–3 h for a single run of the measurements. Viability of the chemical etching as a pre-treatment procedure applicable to industrial-scale materials would require their long-term stability evaluation. The potential values were corrected for the solution resistance, which was measured using electrochemical impedance spectroscopy [47]. Such obtained pairs of steady-state I and IR-drop corrected E values were used to prepare Tafel plots for both types of materials and both types of pre-treatments. For consistency and ease of comparison of our Tafel plots with those reported in the literature, the Tafel plots are shown as a graph of the overpotential (η, $\eta = E_f - 0.00$ V) as a function of log j, where $j = I/A_r$. The experimental approach applied to the determination of A_r is described in detail elsewhere [47]. The specific surface area (A_s) of the as-received and chemically etched Ni foams were found to be 154.5 and 234.0 cm^2 g^{-1}, respectively. The electrochemical experiments were carried out using EG&G PAR263 and 263A potentiostats and a PAR5210 lock-in amplifier. The data were collected and treated using PAR PowerCV and PowerSine software packages. Constant temperature (T) values were maintained by using a Haake W13 bath, a Haake C10 circulator, and a Haake EK20 chiller [54, 59]. SEM and XPS analyses were carried out using a VG Scientific Microlab 310 ultrahigh-vacuum (UHV) surface analysis system with an Al X-ray source (Department of Chemistry, Queen's University) and a LEO 435VP scanning electron microscope (Faculty of Chemistry, University of Warsaw).

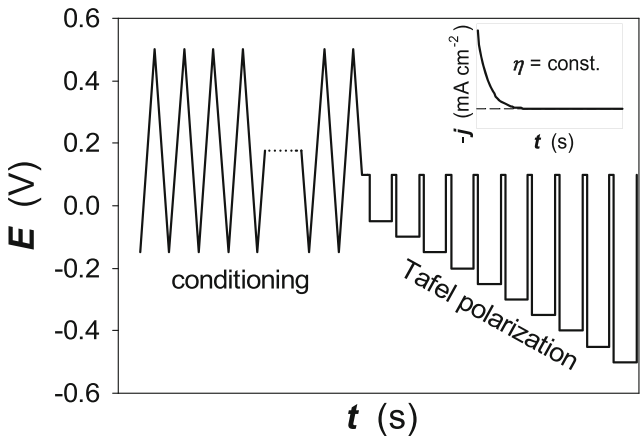

Fig. 4 Program applied to obtain steady-state Tafel polarization curves for the hydrogen evolution reaction at Ni materials. The inset shows a typical current density, j, versus time, t, transient recorded until a steady-state current density is established

Results and Discussion

Tafel Plots at the Room Temperature

Figure 5 presents four Tafel plots for the polished Ni rod, chemically etched Ni rod, as-received Ni foam, and chemically etched Ni foam at the room temperature. All four plots reveal linearity over the entire overpotential range, which facilitates the determination of the values of j_o and b, which are summarized in Table 1. In the case of the Ni foams, the

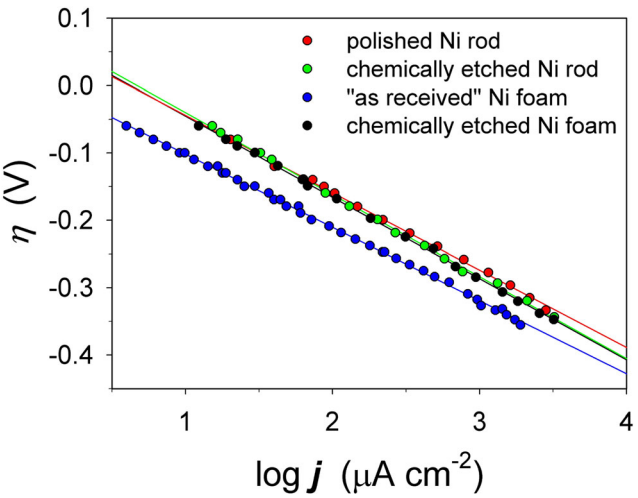

Fig. 5 Steady-state Tafel polarization plots (η versus log j) for the hydrogen evolution reaction in the $-0.05\ \text{V} \le \eta \le -0.35$ V overpotential range and at the temperature of $T = 293$ K in 0.50 M aqueous KOH taking place at the polished Ni rod, the chemically etched Ni rod, the as-received Ni foam, and the chemically etched Ni foam

Table 1 Tafel slope (b), exchange current density (j_o), specific exchange current density ($j_{o,s}$), and apparent activation energy ($E_{a,app}$) for the HER at different Ni materials in 0.50 M aqueous KOH solution. The values of b, j_o, and $j_{o,s}$ are reported for $T = 293$ K; reported values are the average of at least three separate measurements

Electrode material	b (mV dec^{-1})	j_o (μA cm^{-2})	$j_{o,s}$ (mA g^{-1})	$E_{a,app}$ (kJ mol^{-1})
Polished Ni rod	115 ± 2	4.2 ± 1.0	–	40 ± 3
Chemically etched Ni rod	125 ± 5	4.7 ± 1.1	–	42 ± 3
As-received Ni foam	108 ± 6	1.2 ± 0.3	0.18 ± 0.05	47 ± 5
Chemically etched Ni	123 ± 4	4.1 ± 1.0	0.96 ± 0.17	42 ± 3

exchange current density is also reported per gram of the material (mA g^{-1}); we refer to it as the *specific exchange current density* and use the symbol $j_{o,s}$. The conversion from j_o to $j_{o,s}$ is achieved using Eq. 1:

$$j_{o,s} = j_o \times A_s \tag{1}$$

It is important to mention that because the chemical etching dissolves the topmost surface layers of the Ni foam samples, the value of A_s for the etched Ni foam is different from that for the as-received one not only due to surface roughening but also due to a change in the sample mass [47]. All values of the Tafel slope are in the 108–125-mV dec^{-1} range, with the lowest values obtained for the as-received Ni foam and the highest one for the chemically etched electrodes (interestingly, both chemically etched materials reveal practically the same value of b). Our range of the Tafel slope values is in good agreement with previously reported results for Ni materials [18–30]. The values of j_o for the polished Ni rod, chemically etched Ni rod, and chemically etched Ni foam are very similar. This behavior is expected because the pre-treatment procedures generate surfaces which are mostly metallic [47]. These values agree with those reported in the literature for metallic bulk Ni materials [17, 18, 40] and are slightly smaller than the value of 6.3 μA cm^{-2} reported in the electrochemical volcano plot [17, 53]. A significantly smaller value of j_o is obtained for the as-received Ni foam; this is expected because a majority of its surface is oxidized [47]. This value is in good agreement with those reported in the literature for as-received Ni foam materials [46]. It is important to emphasize that the chemical etching removes the surface oxide layer and increases the microscopic and nanoscopic surface roughness of the Ni foam. For this reason, the value of j_o increases by a factor of 3.4. The chemical etching increases the values of $j_{o,s}$ by a factor of 5.3, thus significantly more than the value of j_o.

In the case of the Ni foam samples, the experimentally determined values of the Tafel slope are both lower (the as-received Ni foam) and higher (the chemically etched Ni foam) than the theoretical value of 116 mV dec^{-1} (Table 1). These two types of behavior suggest that the experimental values of the Tafel slop are related mainly to the surface chemical state and the micro- and nanoscopic surface morphology rather than being due to the presence of open pores. Thus, the departure from the theoretical behavior cannot be solely attributed to the macro-porous structure of these materials [63] but to the chemical and physical states of their surfaces.

Temperature-Dependent Tafel Plots

In order to further examine the influence of the surface pre-treatment of Ni materials on the kinetics of the HER, we recorded Tafel plots at different temperatures and used these plots to determine the apparent activation energy ($E_{a,app}$) of the rate-determining step. Figure 6a–d presents Tafel plots for the four materials acquired at different temperatures in the 277 K ≤ T ≤ 308 K range (the temperature values are not necessarily the same in all four plots). In the case of each material, the results reveal one linear relationship for the entire overpotential range and for the entire set of temperatures. These plots were used to calculate the values of j_o and b at a given temperature for each of the Ni materials. In the case of a single electron transfer being the rate-determining step of the two-electron reduction of water to hydrogen molecule, the slope of the Tafel plot is expressed by Eq. 2 that indicates that it should depend linearly on T:

$$b = \frac{2.303 \times R \times T}{\alpha \times F} \tag{2}$$

where α is the charge transfer coefficient (here, it is assumed to be $\alpha = 0.500$), R is the gas constant, and F is the Faraday constant. In the case of $T = 293$ K, $b = 116$ mV dec^{-1} and the experimental value of b obtained for the polished Ni rod practically matches this value (Fig. 5 and Table 1). In the case of the chemically etched Ni rod and Ni foam, the values of b are slightly higher (125 and 123 mV dec^{-1}, respectively) than the theoretical value. On the other hand, in the case of the as-received Ni foam, the value of b (108 mV dec^{-1}) is lower than the theoretical one.

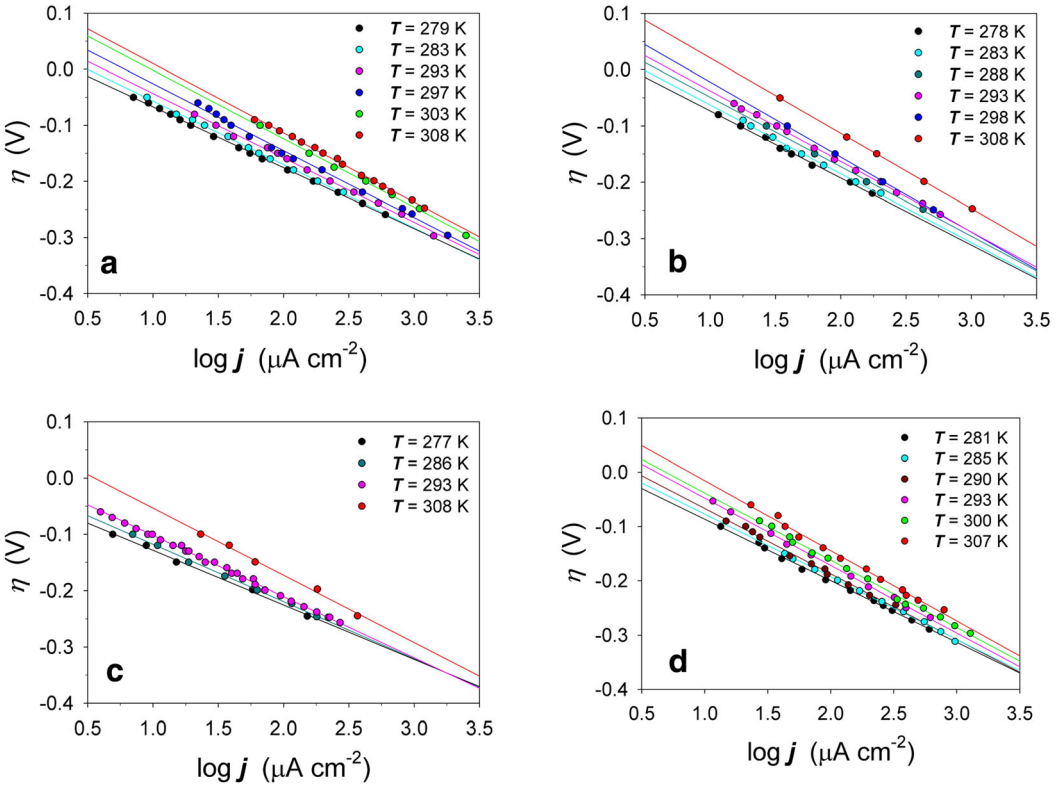

Fig. 6 Steady-state Tafel polarization plots (η versus log j) for the hydrogen evolution reaction in the 277 K ≤ T ≤ 308 K temperature range in 0.50 M aqueous KOH taking place at **a** the polished Ni rod, **b** the chemically etched Ni rod, **c** the as-received Ni foam, and **d** the chemically etched Ni foam

Figure 7a–d presents plots of the value of b as a function of T for the four Ni materials. In all instances, the value of b increases as T rises and these relationships are linear within the experimental uncertainty. Our results are in agreement with those reported by other authors, who also observed an increase in the value of b with rising T [18, 37, 39]. In the case of the polished Ni rod (Fig. 7a), the experimentally determined values of b (the black points) are very close to the theoretical ones (the dashed black line), thus indicating that the system can be accurately described by the theoretical equation. In the case of the etched Ni rod (Fig. 7b), the experimentally determined values of b are higher than the theoretical ones. In the case of the as-received Ni foam (Fig. 7c), the experimentally determined values of b are lower than the theoretical ones. Finally, in the case of the chemically etched Ni foam (Fig. 7d), the experimentally determined values of b are higher than the theoretical ones. In Fig. 7a–d, the theoretically expected behavior is represented by the dashed black line. The results shown in Fig. 7b–d indicate that the kinetics of the HER at these Ni material systems cannot be accurately described by the theoretical equation (Eq. 2). It is interesting to observe that the chemically etched Ni rod (Fig. 7b) and chemically etched Ni foam (Fig. 7d) reveal qualitatively the same behavior, although the actual values of b are different. Only in the case of $T = 293$ K are the values of b for the chemically etched Ni rod and chemically etched Ni foam the same within the experimental uncertainty (Table 1).

Figure 8a–d presents plots of the value of ln j_o as a function of T^{-1} for the four materials. In all cases, the values of ln j_o increase with rising T; the plots are linear and the respective correlation coefficient values are $R^2 \geq 0.98$. The existence of a linearity facilitates the determination of the apparent activation energy ($E_{a,app}$) of the rate-determining step using Eq. 3:

$$\ln j_o = -\frac{E_{a,app}}{R \times T} + A \tag{3}$$

where A is the pre-exponential factor. Such determined values of $E_{a,app}$, which are summarized in Table 1, vary from 40 to 47 kJ mol^{-1}. In the case of the polished Ni rod, chemically etched Ni rod, and chemically etched Ni foam, the $E_{a,app}$ values are practically the same and in the 40–42-kJ mol^{-1} narrow range. In the case of the as-received Ni foam, the value of $E_{a,app}$ is 47 kJ mol^{-1} (ca. 15% greater) due to the presence of a surface oxide/hydroxide layer that is expected to have a lower electrocatalytic activity towards the HER than the metallic Ni. It is worthwhile adding that our $E_{a,app}$ values are in good agreement with those reported in the literature [27, 39, 64–66].

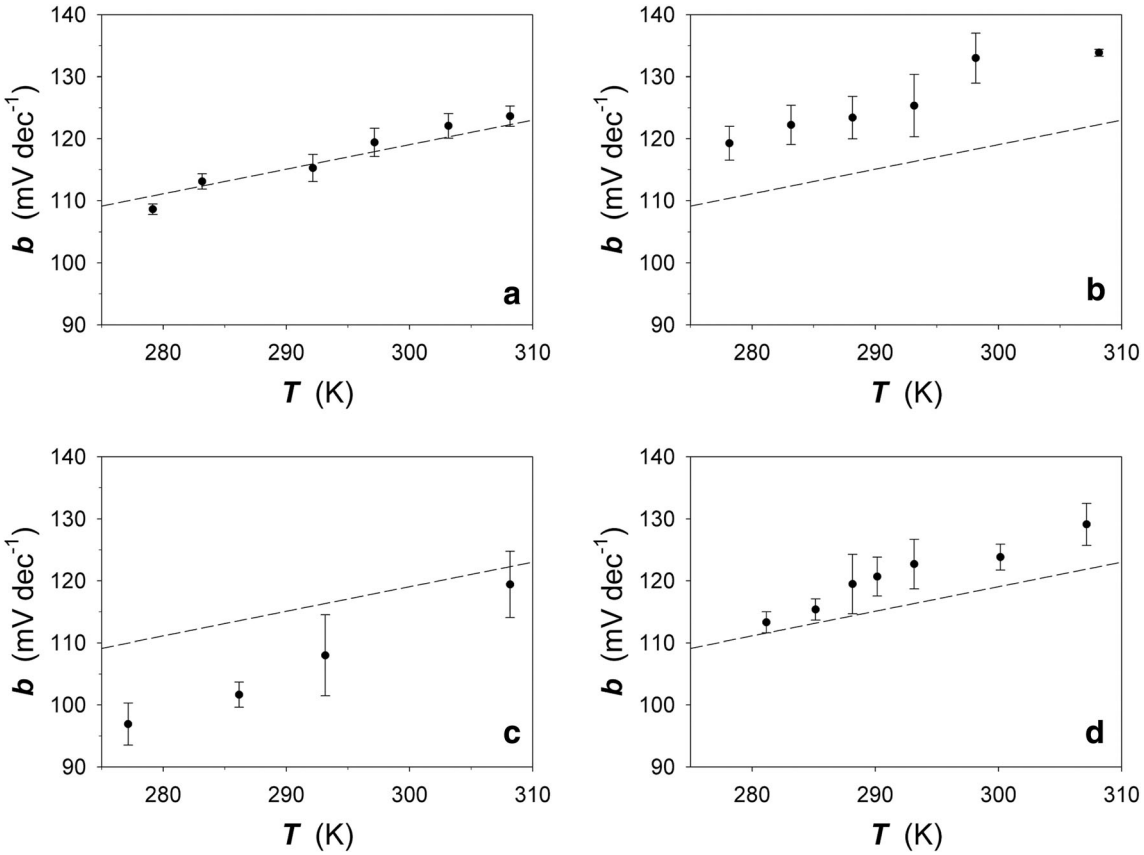

Fig. 7 Values of the Tafel plot slopes, b, for the hydrogen evolution reaction in the 277 K ≤ T ≤ 308 K temperature range in 0.50 M aqueous KOH taking place at **a** the polished Ni rod, **b** the chemically etched Ni rod, **c** the as-received Ni foam, and **d** the chemically etched Ni foam

Discussion of the Significance of the Experimental Results

The above-presented results clearly indicate that the pretreatment of Ni materials has an impact on the kinetics of the HER and that the values of both the Tafel slope (b) and the exchange current density (j_o) are affected. The chemical etching also has a noticeable influence on the apparent activation energy ($E_{a,app}$) in the case of the Ni foam. The most significant changes are observed when the surface oxide/hydroxide layer is removed by the chemical etching. Here, we propose that the surface oxide/hydroxide is catalytically less active than the metallic Ni, because it imposes a barrier to the charge transfer and/or modifies the adsorption behavior of the reaction intermediates and products.

Above, we also report that the chemical etching modifies the values of b and j_o in the case of the Ni rod. Because the Ni rod is polished (it is free of any surface oxide/hydroxide), the modification of the values of b and j_o has to be attributed to other effects. We propose that the chemical etching modifies the surface morphology at the micro- and nano-scale levels. If the changes in the electrocatalytic activity were only due to a change in the real surface area, then the application of the newly determined real surface area of the electrode (the value of A_r after the chemical etching) should produce the same value of j_o, which is not the case. Because the values of b and j_o are different for the Ni rod electrode prior to and after its chemical etching, we propose that the chemical etching introduces a unique nanostructure, which is absent or poorly developed in the case of non-etched Ni material surfaces. This nanostructure modifies the electrocatalytic activity of the material through the creation of active surface sites and modification of the interfacial behavior of the reaction intermediates and products (e.g., surface adsorption, surface diffusion, surface recombination, surface desorption).

The existing literature is inconclusive with regard to the influence of the surface roughness of Ni materials on the kinetics of the HER [25, 33, 34, 45]. However, various authors agree that the surface coverage by the adsorbed intermediate (the overpotential deposited H, H_{OPD}) has a decisive influence on the kinetics of the reaction [31, 33, 41, 44, 67, 68]. Because the surface coverage by H_{OPD} (θ_H) is expected to depend on the electrode surface morphology of Ni materials and because the value of θ_H affects the mechanism and kinetics of the HER, consequently, the kinetics of the HER is expected to depend on the surface morphology of Ni materials. This observation is supported by the results of Conway et al. who studied the kinetics of the HER at monocrystalline Pt electrode [69].

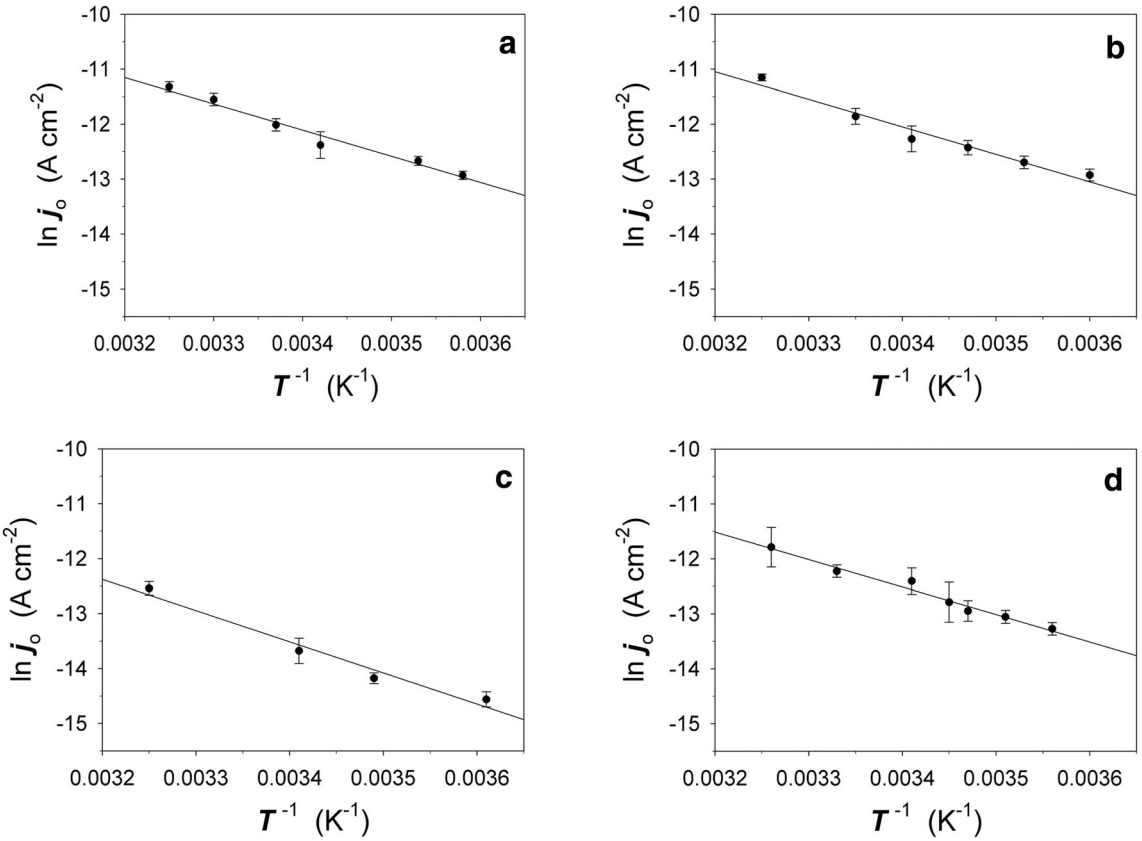

Fig. 8 Plots of log j_o versus T^{-1} for the hydrogen evolution reaction in 0.50 M aqueous KOH taking place at **a** the polished Ni rod, **b** the chemically etched Ni rod, **c** the as-received Ni foam, and **d** the chemically etched Ni foam

Although their materials were atomically flat, the different geometries of surface atoms gave rise to different values of θ_H and the reaction kinetics. Even greater effects are expected in the case of polycrystalline materials, the structure of which is very complex, because they contain ordered and/or disordered grains as well as grain boundaries. In addition, very similar values of $E_{a,app}$ (Table 1) obtained for the polished Ni rod, etched Ni rod, and etched Ni foam suggest that the binding energy of the reaction intermediate (H_{OPD}) is similar in these three cases.

Equation 2 demonstrates that the value of b also depends on the value of the charge transfer coefficient (α). An increase in the value of b upon the Ni material chemical etching or its decrease upon the development of the surface oxide/hydroxide layer can also be attributed to the modification of the value of α while that of the overall reaction pathway remains unchanged. The good agreement between the experimental values of b and the theoretical one for the polished Ni rod (Fig. 7a) indicates that the value of α is very close to the initially accepted value of 0.50. In fact, an average value of α calculated using the experimental data in Fig. 7a is exactly 0.50. We used the same approach and determined the average values of α for the experimental data presented in Fig. 7b–d, and found that α was equal to 0.46 in the case of the etched Ni rod, 0.54 in the case of the as-received Ni foam, and 0.48 in the case of the etched Ni foam. Different than 0.50 values of α for Ni materials were reported by other authors, thus supporting the validity of our findings [19, 64, 70]. In the case of the as-received Ni foam, it is reasonable to assign the increase in the value of α to the existence of the surface oxide/hydroxide layer. Here, we propose that in the case of the etched Ni rod and etched Ni foam, the decrease in the value of α is attributed to the development of new micro- and nanoscopic surface morphological features and associated with their existence phenomena proposed above.

Evaluation of the electrocatalytic activity of a material towards a given electrochemical process (here, the HER) requires the knowledge of both the Tafel slope and the exchange current density, because these two parameters together (through the Butler-Volmer equation) determine the current density at a given overpotential. In the case of the η versus log j plots, the highest electrocatalytic activity is achieved in the case of the highest values of j_o and the lowest value of b. An analysis of data presented in Fig. 4 and Table 1 indicates that although the as-received Ni foam has the lowest value of b, it also has the lowest value of j_o. On the other hand, the chemically etched Ni foam has a higher value of b and a higher value of j_o, as compared to the as-received Ni foam. Despite the increase in b, the chemically etched Ni foam is a better material for the HER in the entire overpotential range reported in this contribution.

Conclusions

The kinetics of the hydrogen evolution reaction at the as-received and chemically etched Ni foams in 0.50 M aqueous KOH solution was studied. The surface chemical composition and morphology of the foam surfaces were characterized using X-ray photoelectron spectroscopy (XPS) and scanning electron microscopy (SEM). Comparative experiments were performed using polished and chemically etched bulk, polycrystalline Ni rods. The as-received Ni foam was mostly covered with a surface oxide/hydroxide layer, which was largely removed by the chemical etching, as confirmed by XPS measurements, while the polished and chemically etched Ni rod was free of any surface oxide. The chemical etching removed the surface oxide/hydroxide layer and modified the surface morphology of the material through the formation of micro- and nanoscopic roughness, as revealed by SEM analysis. The modification of the surface morphology also alters the value of the real surface area of the Ni materials. Both the presence of the surface oxide/hydroxide layer and modification of the surface morphology are found to influence the kinetics of the hydrogen evolution reaction. These are manifested through changes in the value of the slope and the exchange current density of Tafel plots. The pre-treatment of the Ni foams also modifies the value of the apparent activation energy of the rate-determining step of the HER, and this energy is found to be higher in the case of the Ni foam covered with a surface oxide/hydroxide layer. Our results lead to the observation that the kinetics of the HER at Ni foams depends on its surface chemical state and the surface micro- and nano-morphology but does not depend on the macroscopic porosity.

Acknowledgements We acknowledge the financial support from the NSERC of Canada and Queen's University and collaboration with VALE (formerly Vale-Inco). M. Grdeń acknowledges a leave of absence from Warsaw University. This research was conducted as part of the Engineered Nickel Catalysts for Electrochemical Clean Energy project administered from Queen's University and supported by Grant No. RGPNM 477963-2015 under the Natural Sciences and Engineering Research Council of Canada (NSERC) Discovery Frontiers Program.

References

1. A. Czerwiński, M. Żelazowska, Electrochemical behavior of lead dioxide deposited on reticulated vitreous carbon (RVC). J Power Sources **64**(1-2), 29–34 (1997)
2. Z. Rogulski, A. Czerwiński, Cathode modification in the Leclanché cell. J Solid State Electrochem **7**(2), 118–121 (2003)
3. J. van Drunen, B.K. Pilapil, Y. Makonnen, D. Beauchemin, B.D. Gates, G. Jerkiewicz, Electrochemically active nickel foams as support materials for nanoscopic platinum electrocatalysts. ACS Appl Mater Interfaces **6**(15), 12046–12061 (2014)
4. J. Wang, Reticulated vitreous carbon—a new versatile electrode material. Electrochim Acta **26**(12), 1721–1726 (1981)
5. C. Ouyang, X. Wang, C. Wang, X. Zhang, J. Wu, Z. Ma, S. Dou, S. Wang, Hierarchically porous Ni3S2 nanorod array foam as highly efficient electrocatalyst for hydrogen evolution reaction and oxygen evolution reaction. Electrochim Acta **174**, 297–301 (2015)
6. M. Schalenbach, A.R. Zeradjanin, O. Kasian, S. Cherevko, K.J.J. Mayrhofer, Int J Electrochem Soc **13**, 1173 (2018)
7. S. Fiameni, I. Herraiz-Cardona, M. Musiani, V. Pérez-Herranz, L. Vázquez-Gómez, E. Verlato, The HER in alkaline media on Pt-modified three-dimensional Ni cathodes. Int J Hydrogen Energy **37**(14), 10507–10516 (2012)
8. K. Zhang, J. Li, W. Liu, J. Liu, C. Yan, Electrocatalytic activity and electrochemical stability of Ni–S/CeO2 composite electrode for hydrogen evolution in alkaline water electrolysis. Int J Hydrogen Energy **41**(48), 22643–22651 (2016)
9. J. van Drunen, T.W. Napporn, B. Kokoh, G. Jerkiewicz, Electrochemical oxidation of isopropanol using a nickel foam electrode. J Electroanal Chem **716**, 120–128 (2014)
10. S. Zamponi, A. Czerwiński, G. Gambini, R. Marassi, Linear sweep voltabsorptometry with a finite diffusion space. J Electroanal Chem **332**(1-2), 63–71 (1992)
11. M. Chotkowski, Extraction of moderate oxidation state technetium species between 30 % tri-n-butyl phosphate and H2SO4/HNO3. J Radioanal Nucl Ch **307**(1), 457–462 (2016)
12. V. Paserin, S. Marcuson, J. Shu, D.S. Wilkinson, CVD technique for Inco nickel foam production. Adv Eng Mater **6**(6), 454–459 (2004)
13. F. Safizadeh, E. Ghali, G. Houlachi, Electrocatalysis developments for hydrogen evolution reaction in alkaline solutions—a review. Int J Hydrogen Energy **40**(1), 256–274 (2015)
14. K. Zeng, D. Zhang, Recent progress in alkaline water electrolysis for hydrogen production and applications. Prog Energy Combust **36**(3), 307–326 (2010)
15. Z. Xie, P. He, L. Du, F. Dong, K. Dai, T. Zhang, Comparison of four nickel-based electrodes for hydrogen evolution reaction. Electrochim Acta **88**, 390–394 (2013)
16. R.M. Abouatallah, D.W. Kirk, S.J. Thorpe, J.W. Graydon, Reactivation of nickel cathodes by dissolved vanadium species during hydrogen evolution in alkaline media. Electrochim Acta **47**(4), 613–621 (2001)
17. B.E. Conway, G. Jerkiewicz, Relation of energies and coverages of underpotential and overpotential deposited H at Pt and other metals to the 'volcano curve' for cathodic H2 evolution kinetics. Electrochim Acta **45**(25-26), 4075–4083 (2000)
18. S.A.S. Machado, L.A. Avaca, The hydrogen evolution reaction on nickel surfaces stabilized by H-absorption. Electrochim Acta **39**(10), 1385–1391 (1994)
19. A. Lasia, A. Rami, Kinetics of hydrogen evolution on nickel electrodes. J Electroanal Chem **294**(1-2), 123–141 (1990)
20. J. Divisek, Determination of the kinetics of hydrogen evolution by analysis of the potential-current and potential-coverage curves. J Electroanal Chem **214**(1-2), 615–632 (1986)
21. O. Savadogo, The hydrogen evolution reaction in alkaline medium on nickel modified with W042− or Mo042−. Electrochim Acta **37**(8), 1457–1459 (1992)
22. H.J. Miao, D.L. Piron, Composite-coating electrodes for hydrogen evolution reaction. Electrochim Acta **38**(8), 1079–1085 (1993)
23. I.J. Brown, S. Sotiropoulos, J Appl Electrochem **30**(1), 107–111 (2000)
24. N. Krstajić, M. Popović, B. Grgur, On the kinetics of the hydrogen evolution reaction on nickel in alkaline solution. J Electroanal Chem **512**(1-2), 27–35 (2001)
25. T. Benameur, R. Yavari, R. Durand, Electrocatalytic behavior of non-equilibrium b.c.c. nickel. Mater Sci Eng A **181-182**, 1145–1149 (1994)

26. J.Y. Huot, Hydrogen evolution and interface phenomena on a nickel cathode in 30 w/o KOH. J Electrochem Soc **136**(7), 1933 (1989)
27. A.G. Oshchepkov, A. Bonnefont, V.N. Parmon, E.R. Savinova, On the effect of temperature and surface oxidation on the kinetics of hydrogen electrode reactions on nickel in alkaline media. Electrochim Acta **269**, 111–118 (2018)
28. A. Kellenberger, N. Vaszilcsin, W. Brandl, N. Duteanu, Kinetics of hydrogen evolution reaction on skeleton nickel and nickel–titanium electrodes obtained by thermal arc spraying technique. Int J Hydrogen Energy **32**(15), 3258–3265 (2007)
29. M.A.V. Devanathan, M. Selvaratnam, Mechanism of the hydrogen-evolution reaction on nickel in alkaline solutions by the determination of the degree of coverage. Trans Faraday Soc **56**, 1820 (1960)
30. I. Bianchi, E. Guerrini, S. Trasatti, Electrocatalytic activation of Ni for H2 evolution by spontaneous deposition of Ru. Chem Phys **319**(1-3), 192–199 (2005)
31. Z. Liang, H.S. Ahn, H.S., A.J. Bard, A study of the mechanism of the hydrogen evolution reaction on nickel by surface interrogation scanning electrochemical microscopy. J Am Chem Soc **139**(13), 4854–4858 (2017)
32. M.F. Kibria, M.S. Mridha, A.H. Khan, Electrochemical studies of a nickel electrode for the hydrogen evolution reaction. Int J Hydrogen Energy **20**(6), 435–440 (1995)
33. G. Kreysa, B. Håkansson, P. Ekdunge, Kinetic and thermodynamic analysis of hydrogen evolution at nickel electrodes. Electrochim Acta **33**(10), 1351–1357 (1988)
34. A.P. Brown, M. Krumpelt, R.O. Loutfy, N.P. Yao, The effect of surface roughness on the hydrogen evolution reaction kinetics with mild steel and nickel cathodes. Electrochim Acta **27**(5), 557–560 (1982)
35. D.S. Hall, C. Bock, B.R. MacDougall, The electrochemistry of metallic nickel: oxides, hydroxides, hydrides and alkaline hydrogen evolution. J Electrochem Soc **160**(3), F235–F243 (2013)
36. A.C. Chialvo, M.R. Gennero de Chialvo, Electrocatalytic activity of nickel black electrodes for the hydrogen evolution reaction in alkaline solutions. J Appl Electrochem **21**(5), 440–445 (1991)
37. J.O'.M. Bockris, E.C. Potter, The mechanism of hydrogen evolution at nickel cathodes in aqueous solutions. J Chem Phys **20**(4), 614–628 (1952)
38. R. Palaniappan, G.G. Botte, Effect of ammonia on Pt, Ru, Rh, and Ni cathodes during the alkaline hydrogen evolution reaction. J Phys Chem C **117**(34), 17429–17441 (2013)
39. C. González-Buch, I. Herraiz-Cardona, E. Ortega, J. García-Antón, V. Pérez-Herranz, Synthesis and characterization of macroporous Ni, Co and Ni–Co electrocatalytic deposits for hydrogen evolution reaction in alkaline media. Int J Hydrogen Energy **38**(25), 10157–10169 (2013)
40. M.A. McArthur, L. Jorge, S. Coulombe, S. Omanovic, Synthesis and characterization of 3D Ni nanoparticle/carbon nanotube cathodes for hydrogen evolution in alkaline electrolyte. J Power Sources **266**, 365–373 (2014)
41. L. Angely, G. Bronoel, G. Peslerbe, Relation between nickel crystalline structures and their electrocatalytic properties. J Electroanal Chem **96**(2), 203–208 (1979)
42. J.L. Weininger, M.W. Breiter, Hydrogen evolution and surface oxidation of nickel electrodes in alkaline solution. J Electrochem Soc **111**(6), 707 (1964)
43. D.M. Soares, O. Teschke, I. Torriani, Hydride effect on the kinetics of the hydrogen evolution reaction on nickel cathodes in alkaline media. J Electrochem Soc **139**(1), 98 (1992)
44. Y. Choquette, L. Brossard, A. Lasia, H. Ménard, Investigation of hydrogen evolution on Raney-Nickel composite-coated electrodes. Electrochim Acta **35**(8), 1251–1256 (1990)
45. C.A. Marozzi, A.C. Chialvo, Development of electrode morphologies of interest in electrocatalysis. Electrochim Acta **46**(6), 861–866 (2001)
46. B. Pierozynski, T. Mikolajczyk, I.M. Kowalski, Hydrogen evolution at catalytically-modified nickel foam in alkaline solution. J Power Sources **271**, 231–238 (2014)
47. M. Grdeń, M. Alsabet, G. Jerkiewicz, Surface science and electrochemical analysis of nickel foams. ACS Appl Mater Interfaces **4**(6), 3012–3021 (2012)
48. A.F.B. Barbosa, V.L. Oliveira, J. van Drunen, G. Tremiliosi-Filho, Ethanol electro-oxidation reaction using a polycrystalline nickel electrode in alkaline media: temperature influence and reaction mechanism. J Electroanal Chem **746**, 31–38 (2015)
49. J. van Drunen, A.F.B. Barbosa, G. Tremiliosi-Filho, The formation of surface oxides on nickel in oxalate-containing alkaline media. Electrocatalysis **6**(5), 481–491 (2015)
50. D.S. Hall, C. Bock, B.R. MacDougall, An oxalate method for measuring the surface area of nickel electrodes. J Electrochem Soc **161**(12), H787–H795 (2014)
51. A. Kellenberger, N. Vaszilcsin, W. Brandl, J Solid State Electrochem **11**, 84 (2007)
52. M.J. Gira, K.P. Tkacz, J.R. Hampton, Physical and electrochemical area determination of electrodeposited Ni, Co, and NiCo thin films. Nano Converg **3**(1), 6–1 (2016)
53. J.K. Nørskov, T. Bligaard, A. Logadottir, J.R. Kitchin, J.G. Chen, S. Pandelov, U. Stimming, Trends in the exchange current for hydrogen evolution. J Electrochem Soc **152**(3), J23 (2005)
54. M. Alsabet, M. Grdeń, G. Jerkiewicz, Electrochemical growth of surface oxides on nickel. Part 1: formation of α-Ni(OH)2 in relation to the polarization potential, polarization time, and temperature. Electrocatalysis **2**(4), 317–330 (2011)
55. P. Zoltowski, The capacity of monocrystalline nickel electrode in potassium hydroxide solution at low hydrogen overpotentials. Electrochim Acta **38**(14), 2129–2133 (1993)
56. J. van Drunen, B. Brandy Kinkead, M.C.P. Wang, E. Sourty, B.D. Gates, G. Jerkiewicz, A.C.S. Appl, Comprehensive structural, surface-chemical and electrochemical characterization of nickel-based metallic foams. Mater. Inter. **5**(14), 6712–6722 (2013)
57. M.C. Biesinger, B.P. Payne, A.P. Grosvenor, L.W.M. Lau, A.R. Gerson, R.S.C. Smart, Resolving surface chemical states in XPS analysis of first row transition metals, oxides and hydroxides: Cr, Mn, Fe, Co and Ni. Appl Surf Sci **257**(7), 2717–2730 (2011)
58. M. Alsabet, M. Grdeń, G. Jerkiewicz, Electrochemical growth of surface oxides on nickel. Part 2: formation of β-Ni(OH)2 and NiO in relation to the polarization potential, polarization time, and temperature. Electrocatalysis **5**(2), 136–147 (2014)
59. M. Alsabet, M. Grdeń, G. Jerkiewicz, Electrochemical growth of surface oxides on nickel. Part 3: formation of β-NiOOH in relation to the polarization potential, polarization time, and temperature. Electrocatalysis **6**(1), 60–71 (2015)
60. B. Beden, A. Bewick, The anodic layer on nickel in alkaline solution: an investigation using in situ IR spectroscopy. Electrochim Acta **33**(11), 1695–1698 (1988)
61. M. Dmochowska, A. Czerwiński, Behavior of a nickel electrode in the presence of carbon monoxide. J Solid State Electrochem **2**(1), 16–23 (1998)
62. S. Hrapovic, B.L. Luan, M. D'Amours, G. Vatankhah, G. Jerkiewicz, Morphology, chemical composition, and electrochemical characteristics of colored titanium passive layers. Langmuir **17**(10), 3051–3060 (2001)
63. A. Lasia, Hydrogen evolution/oxidation reactions on porous electrodes. J Electroanal Chem **454**(1-2), 115–121 (1998)

64. H. Wendt, V. Plzak, Electrocatalytic and thermal activation of anodic oxygen- and cathodic hydrogen-evolution in alkaline water electrolysis. Electrochim Acta **28**(1), 27–34 (1983)
65. B.E. Conway, L. Bai, H2 evolution kinetics at high activity Ni-Mo-Cd electrocoated cathodes and its relation to potential dependence of sorption of H☆. Int J Hydrogen Energy **11**(8), 533–540 (1986)
66. B. Pierozynski, T. Mikolajczyk, Int J Electrochem Soc **10**, 10454 (2015)
67. G. Jerkiewicz, Electrochemical Hydrogen Adsorption and Absorption. Part 1: Under-potential Deposition of Hydrogen. Electrocatalysis **1**(4), 179–199 (2010)
68. G. Jerkiewicz, Hydrogen sorption ATIN electrodes. Prog Surf Sci **57**(2), 137–186 (1998)
69. B.E. Conway, J. Barber, S. Morin, Comparative evaluation of surface structure specificity of kinetics of UPD and OPD of H at single-crystal Pt electrodes. Electrochim Acta **44**(6-7), 1109–1125 (1998)
70. N. Krstajić, M. Popović, B. Grgur, M. Vojnović, D. Šepa, On the kinetics of the hydrogen evolution reaction on nickel in alkaline solution. J Electroanal Chem **512**(1-2), 16–26 (2001)